Controller Design Challenges for Waterjet Propelled Unmanned Surface Vehicles with Uncertain Drag and Mass Properties

Wilhelm B. Klinger, Ivan Bertaska, José Alvarez and Karl D. von Ellenrieder,
Department of Ocean and Mechanical Engineering
Florida Atlantic University
Dania Beach, Florida
wklinger@fau.edu

***Abstract*— The issues affecting low-level controller design for a wave-adaptive modular class of unmanned surface vehicles (USVs) are presented in the context of supporting the autonomous launch and recovery (ALR) of an Autonomous Underwater Vehicle (AUV) aboard an USV. The ALR of an AUV presents a challenging control problem because control parameters are chosen based on the dynamics of the vehicle, which can change abruptly and significantly when an AUV is jettisoned or docked. Tight control of the vehicle state is required to conduct an underway recovery, with looser requirements for the launch. Knowledge of the vehicle response is important for control system design. A simulation, based on physical modeling and experimental results, was developed to support the design of a low level controller. A cascaded proportional derivative (PD) controller has been implemented in simulation and tested for two dissimilar reference speeds and two payload conditions. The simulation results suggest that an adaptive controller may be necessary to overcome the time-varying nature of USV dynamics during an ALR mission.**

Keywords—Marine Vehicles; System Identification, State-space Methods

I. Introduction & Background

Several defense oriented missions in which Unmanned Surface Vehicles (USVs) could be used, include, but are not limited to: asset protection, mine countermeasures, area denial, and target tracking [1]. A topic of particular interest is the launch and recovery of an Autonomous Underwater vehicle (AUV) by an USV. By combining an AUV and USV for a designated mission, longer range operations with less human support can be achieved. Reducing the need for human oversight during a mission is a desirable outcome of automation, especially when the mission environment could present a danger to human life.

To date, the retrieval of an AUV is a manned operation. It has never, to the knowledge of the authors, been implemented fully autonomously. While the autonomous launch of an unmanned underwater vehicle from an unmanned surface vehicle has been accomplished [2], to the authors' knowledge autonomous retrieval has not been achieved to date. Hydroid, the maker of the REMUS AUV series, has developed a way to conduct an unmanned underway docking of a REMUS AUV [4]. However, the actual launch and recovery is designated as a manned operation, with the docking sequence a means of decreasing the frequency of launch and recovery.

This paper describes the challenges of controlling an USV during the ALR of an AUV and reviews the capabilities that have been developed to date. A method for modeling a twin-hulled wave-adaptive class of USVs is presented. Initial system identification test results are presented alongside simulation results to verify the model. Finally, a control case study of a pair of cascaded PD controllers is presented to illustrate the challenges in controlling a twin-hulled wave-adaptive class of USVs experiencing extreme changes in mass properties during operation. Simulation results are presented with the case study.

II. Approach to Control Design

From a surface vehicle control aspect, the challenge of conducting an ALR mission lies in designing a controller which is insensitive to drastic changes in the displacement and drag properties of the USV. The reason changing drag properties would affect the controller's performance lies in how control inputs are determined. Typically, a controller is fed information in the form of an error between a desired state variable and the measured/estimated state variable. Using this information, the controller calculates the required output that will drive the vehicle state towards its desired state. The calculations are heavily dependent on the dynamic properties of the specific platform. For example, the USV under consideration by the authors is a 14 foot (4.3 m) Wave-Adaptive Modular Vehicle (WAM-V 14) weighing 150 kg. The AUV is a REMUS 100, which weighs 38.5 kilograms (kg) in air. The maximum rated payload of the USV is 114 kg. Accordingly, the ALR system can weigh no more than 75.5 kg. The lightship mass will consist of the vehicle and ALR system (combined maximum of 225 kg) and the full displacement mass will be up to 264 kg. The minimum change in displacement will be 17% of the full USV displacement, and this percentage will increase as the mass of the ALR mechanical system decreases. The stock USV is rated for a maximum payload of 76% of its total weight.

Consider the lightship condition when the speed error is 1 m/s. A non-adaptive controller designed for this vehicle condition will compute the additional waterjet impeller shaft speed required from each motor to increase the forward speed

978-0-933957-40-4

of the vehicle by 1 m/s. If the control law is accurate and there are no additional forces acting on the vehicle (e.g. wind, current, waves), the vehicle's speed will increase by 1 m/s with the new waterjet shaft speed commands.

Consider now the full displacement condition, where the AUV is aboard the USV. The vehicle now weighs approximately 17% more and the controller will be actuating against a higher error signal because the control action is based on the dynamics of the previous vehicle condition. It would be expected that the time response from start up to steady state might become unacceptable if the vehicle's maneuvering characteristics change significantly due to the change in mass.

The new response of the vehicle to motor commands will be dependent on the drag of the vehicle, which is affected by the draft of the hull. In addition the center of gravity could shift during ALR operations. The same shortcomings would be relevant when the vehicle is required to correct a heading error, where the required yaw moment is a function of the vehicle moment of inertia about the heave axis as well as the hydrodynamic resistance to rotation experienced by the vehicle. This scenario of variable system response suggests that an adaptive element be incorporated within the vehicle's low-level controller. Slotine [5] discusses several reasons for using adaptive control, one of which is a situation where the plant changes while the controller is in operation. This situation requires a continuous 'redesign' of the controller to avoid inaccuracy or instability of the control system.

A. Vehicle Modeling

A three degree of freedom (surge, sway, and yaw) vehicle model is used, as presented in [6], where

$$\boldsymbol{M\dot{v}} + \boldsymbol{C(v)v} + \boldsymbol{D(v)v} = \boldsymbol{\tau} \quad (1)$$

$$\boldsymbol{\dot{\eta}} = (\dot{x}\,\dot{y}\,\dot{\psi})^T, \quad (2)$$

and

$$\boldsymbol{v} = (u\,v\,r)^T. \quad (3)$$

Here, the vector $\boldsymbol{\dot{\eta}}$ describes the vehicle linear North ($\dot{x}$), East ($\dot{y}$), and Z-axis angular velocities ($\dot{\psi}$) in an inertial reference frame (x, y, ψ) and $\boldsymbol{v}$ contains the vehicle surge (u), sway (v) and yaw velocities (r) in the body fixed frame (x_b, y_b, ψ). Figure 1 illustrates the two coordinate systems and the motor forces acting on the vehicle.

$\boldsymbol{J(\eta)}$ is the transformation matrix for converting from body-fixed to earth-fixed frames:

$$\boldsymbol{J(\eta)} = \begin{bmatrix} \cos\psi & -\sin\psi & 0 \\ \sin\psi & \cos\psi & 0 \\ 0 & 0 & 1 \end{bmatrix}. \quad (4)$$

$\boldsymbol{M}$ is a mass matrix that is the sum of a rigid body mass matrix and an added mass matrix:

$$\boldsymbol{M} = \boldsymbol{M_{RB}} + \boldsymbol{M_A} = \begin{bmatrix} m - X_{\dot{u}} & -X_{\dot{v}} & -my_G - X_{\dot{r}} \\ -X_{\dot{u}} & m - Y_{\dot{v}} & mx_G - Y_{\dot{r}} \\ -my_G - N_{\dot{u}} & mx_G - N_{\dot{v}} & I_z - N_{\dot{r}} \end{bmatrix}. \quad (5)$$

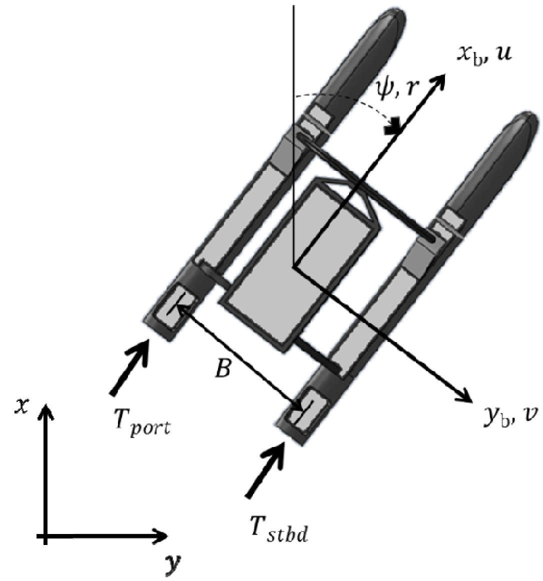

Figure 1. Surface Vehicle Planar Dynamic Motions

$\boldsymbol{C(v)}$ is a Coriolis matrix, which includes the sum of a rigid body and added mass matrix:

$$\boldsymbol{C(v)} = \boldsymbol{C_{RB}} + \boldsymbol{C_A} = \begin{bmatrix} 0 & 0 & -m(x_G r + v) \\ 0 & 0 & -m(y_G r - u) \\ m(x_G r + v) & m(y_G r - u) & 0 \end{bmatrix} + \begin{bmatrix} 0 & 0 & -\left(Y_{\dot{v}} v + \frac{Y_{\dot{r}} + N_{\dot{v}}}{2} r\right) \\ 0 & 0 & X_{\dot{u}} u \\ Y_{\dot{v}} v + \frac{Y_{\dot{r}} + N_{\dot{v}}}{2} r & -X_{\dot{u}} u & 0 \end{bmatrix}. \quad (6)$$

Note that the current model designates the body-fixed origin at the center of gravity and assumes horizontal symmetry, making the values x_G and y_G equal zero. $\boldsymbol{D(v)}$ is the summation of linear and nonlinear drag matrices:

$$\boldsymbol{D(v)} = \boldsymbol{D} + \boldsymbol{D_n} \quad (7)$$

where,

$$\boldsymbol{D} = -\begin{bmatrix} X_u & 0 & 0 \\ 0 & Y_v & Y_v \\ 0 & N_v & N_r \end{bmatrix} \quad (8)$$

and,

$$\boldsymbol{D_n} = -\begin{bmatrix} X_{u|u|}|u| & 0 & 0 \\ 0 & Y_{v|v|}|v| + Y_{|r|v}|r| & Y_{|v|r}|v| + Y_{r|r|}|r| \\ 0 & N_{v|v|}|v| + N_{|r|v}|r| & N_r|v| + N_{|r|r}|r| \end{bmatrix}. \quad (9)$$

The terms in the drag and Coriolis matrices are nomenclature for representing a force or moment created by motion in a specific degree of freedom, where X and Y correspond to force in the x and y directions, respectively, and N denotes a moment about the Z-axis. The subscript on each coefficient denotes the cause of the force/moment. For example, X_u can be read as, ‘force in the x-direction due to forward velocity.’ Coefficients with two different subscripts denote nonlinear coupling terms, and two of the same subscripts imply the coefficient belongs to a quadratic term.

Finally, $\boldsymbol{\tau}$ is a vector that contains the sum of all other forces and moments acting on the vehicle, which for the twin-hull waterjet propelled vehicle under consideration, is only the port and starboard thrusters:

$$\tau = \begin{bmatrix} \left(T_{port} + T_{stbd}\right) \\ 0 \\ \left(T_{port} - T_{stbd}\right) * \frac{B}{2} \end{bmatrix}. \qquad (10)$$

Here T denotes the thrust from each respective motor and B is the side hull separation (hull centerline to hull centerline).

The conversion from the control signal, RPM, to motor thrust is modeled in the simulation linearly with the equation:

$$T = \frac{T_{max}}{RPM_{max}} * RPM, \qquad (11)$$

where thrust is denoted by T. T_{max} stands for the maximum thrust of the motor, RPM is motor speed in revolutions per minute, and RPM_{max} denotes the maximum RPM rating of the motor. For the WAM-V 14, the nominal T_{max} and RPM_{max} is 102 Newtons and $2.2e4$ RPM, respectively. The maximum waterjet thrust was measured via an open-loop bollard pull test.

B. Autonomous Surface Vehicle Identification

As a starting point for system identification, the WAM-V 14 USV was run through a series of open-loop maneuvering tests. The purpose of these tests was to obtain the steady state dynamics of the vehicle [10] and to provide data to aid the initial estimation of the model maneuvering coefficients.

1) Zig-Zag Test

A modified on-water zig-zag test was conducted via human operated remote control as well as using pre-determined open-loop commands supplied via a control box. The traditional zig-zag test specifies rudder commands for a certain heading range [8], but for a vehicle steered using differential thrust the test must be conducted by varying the motor speeds. Motor commands were alternated between 0 and 100% power, with the port and starboard motor commands issued 180° out of phase. Each motor setting was held for 7 seconds. From this test, the vehicle’s maximum yaw rate achieved was found to be 15.6 °/s, whereas for the lightship condition the maximum measured yaw rate was 13.4 °/s. Figure 2 displays the simulated and experimental trajectory of the USV during the zig-zag test for one test case, as well as the time record of yaw rate (2b) and the surge velocity (2c) for several runs of the same test. It can be noted from Figure 2c that the mathematical model currently does not accurately capture the surge motion characteristics of the vehicle during periods of

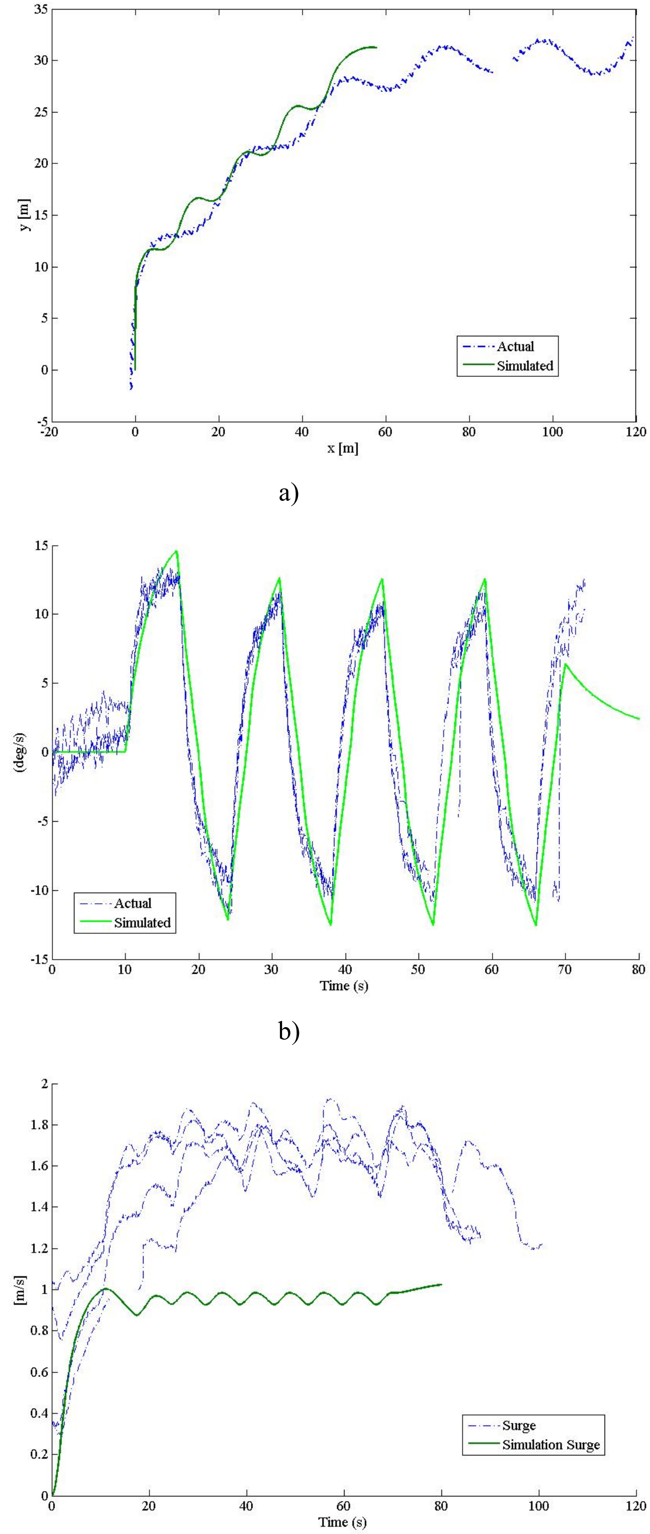

c)

Figure 2. Zigzag maneuvering data. a) Trajectory. b) Yaw rate. c) Surge velocity.

yaw motion. The graph shows that the signals are out of phase however the magnitudes of oscillation and yaw rates match.

The phase issue in Figure 2a is due to the disparity between simulated and actual surge velocities during the zig-zag test.

2) Circle Test

The circle test is conducted by first establishing a steady state condition and then setting one motor to a constant speed and the other to zero. Again, this procedure is necessarily altered from the standard circle test [8]. The vehicle tracks a circular pattern for a minimum of 720 degrees. This test is conducted at several motor speeds for both port and starboard turns.

The full circle test procedure for the un-weighted case is tabulated in Table I with experimental results for circle period at each motor setting, again in the un-weighted case. Figure 3 displays the simulated and actual vehicle surge velocity and yaw rate during the circle test maneuver for the 100% and 80% cases in the lightship condition.

Notice the yaw rate oscillating during the circles which correspond to the vehicle turning into and out of wind varying in speed between 6-7 knots.

Note also that although the circle period decreased by 32% between the 50 and 100% throttle tests, the turning radius only increased by 4%. This implies that the vehicle's turning radius is much more dependent on yaw moment than thrust magnitude.

Table II contains steady state surge velocity and yaw rate values for the USV under both the lightship and full displacement conditions for three motor commands between 80-100%. It can be seen from the surge and yaw rate data that a bias exists between the two motors. The port motor produced a faster turn rate and surge velocity for each of the six runs. Several factors could be the cause of this motor bias. The number of windings on each motor may differ, or the battery sets may have been at different voltages between the two pods. Also, the electronic speed controllers within the pods may be programmed in a way that produces different voltages for the same Pulse Width Modulated (PWM) signal received from the control box.

3) Acceleration Test

Another system identification test conducted was the acceleration test. The vehicle started in a stationary position,

Table I. Open Loop Circle Test Results for the Un-weighted Displacement Case.

Run #	Port Throttle Position (%)	Starboard Throttle Position (%)	Circle Period (s)	Turning Radius (m)
1	25	0	54	-
2	0	25	66	-
3	50	0	45	4.2
4	0	50	41	5.0
5	75	0	40	-
6	0	75	36	-
7	100	0	31	-
8	0	100	29	5.2

[a]**Some position data was corrupted due to sensor issues during testing**

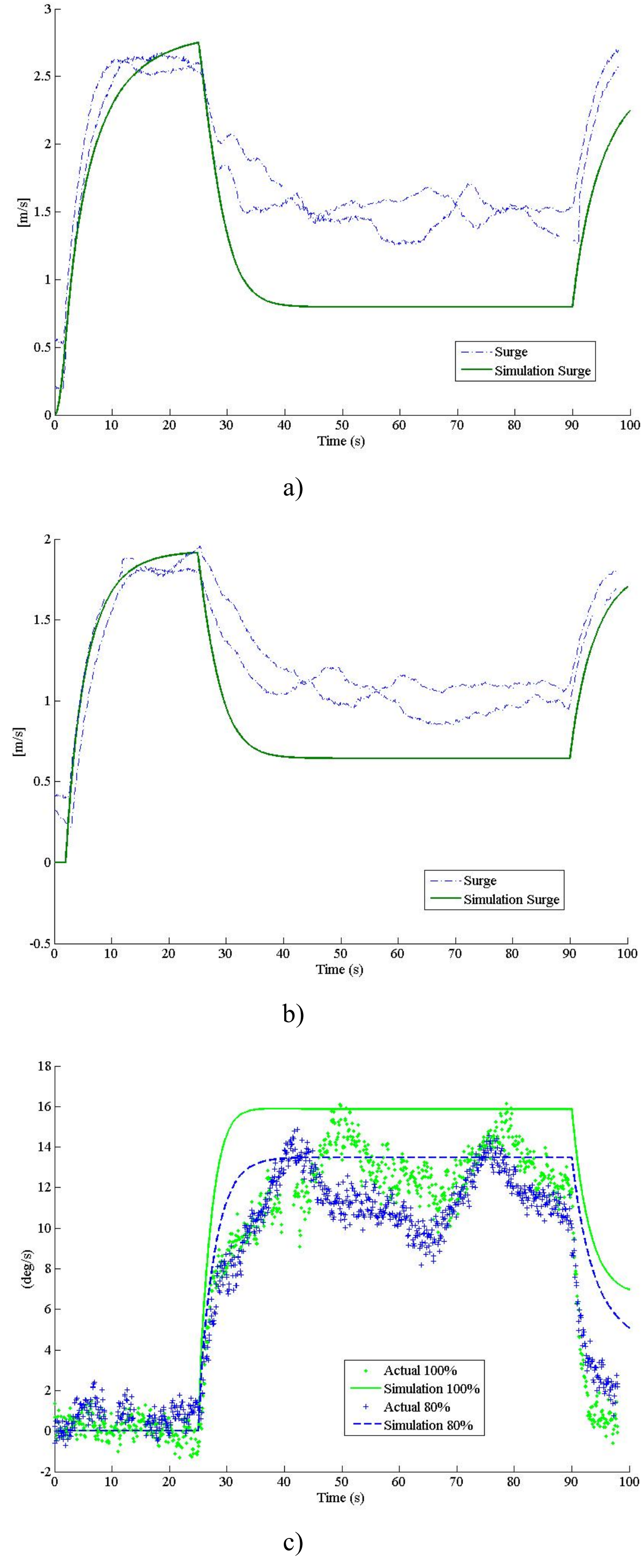

Figure 3. Circle test results. a) 100% motor command. b) 80% motor command. c) Yaw rate for 100% and 80% cases.

with forward, side, and yaw velocity as close to zero as possible, and was accelerated to a constant throttle setting on both motors for 60 seconds. 10-20 seconds after switching the

Table II. Open Loop Circle Test Surge and Yaw Results

Motor Commands (%)		Displacement Condition			
		Lightship		Full Displacement	
Port	Starboard	Turn Rate (deg/s)	Surge (m/s)	Turn Rate (deg/s)	Surge (m/s)
100	0	13.11	1.54	12.71	1.53
90	0	12.59	1.29	10.64	1.19
80	0	11.66	1.12	8.73	0.89
0	100	-11.29	1.46	-11.77	1.27
0	90	-11.16	1.17	-9.93	0.93
0	80	-9.87	0.97	-7.66	0.69

motors off were also logged in order to identify how the vehicle slows down. The test was conducted with throttle speeds ranging from 40-100%. Experimental results for the acceleration test are presented in Table III for both the un-weighted displacement condition and with approximately 70 kg attached along the centerline of the vehicle simulating the lightship condition of the ALR mission.

Figure 4a displays vehicle surge velocity data for the simulated and experimental 100% acceleration tests under the lightship condition, while Figure 4b displays the 80% acceleration case. From the graph it can be seen that the vehicle's full acceleration period is approximately 20 seconds. Data from the half throttle acceleration tests showed a 15 second acceleration period.

By collecting data over a wide range of speeds, forward speed curves were produced for each displacement condition based on the PWM duty cycle integer value that is passed from a PWM generator in the control box to the electronic speed controller in each motor pod that controls the motor speed. The PWM value is the integer that is calculated in the control code because the output must be in a format accepted by the PWM generator. The PWM signal scales linearly with motor throttle percent. By assuming a linear relation between motor commands and PWM duty cycle, the PWM motor command is plotted in Figure 5 for three displacement conditions of the vehicle against steady state cruising velocities. Notice that as the displacement of the pontoon increases from Figure 5a-c that the motor command curve becomes increasingly linear with speed.

Table III. Acceleration Test Results

Vehicle Configuration	Throttle Setting	Peak Acceleration (m/s^2)
Un-Weighted	50%	0.3079
	100%	0.8867
Lightship	50%	0.2200
	100%	0.8244

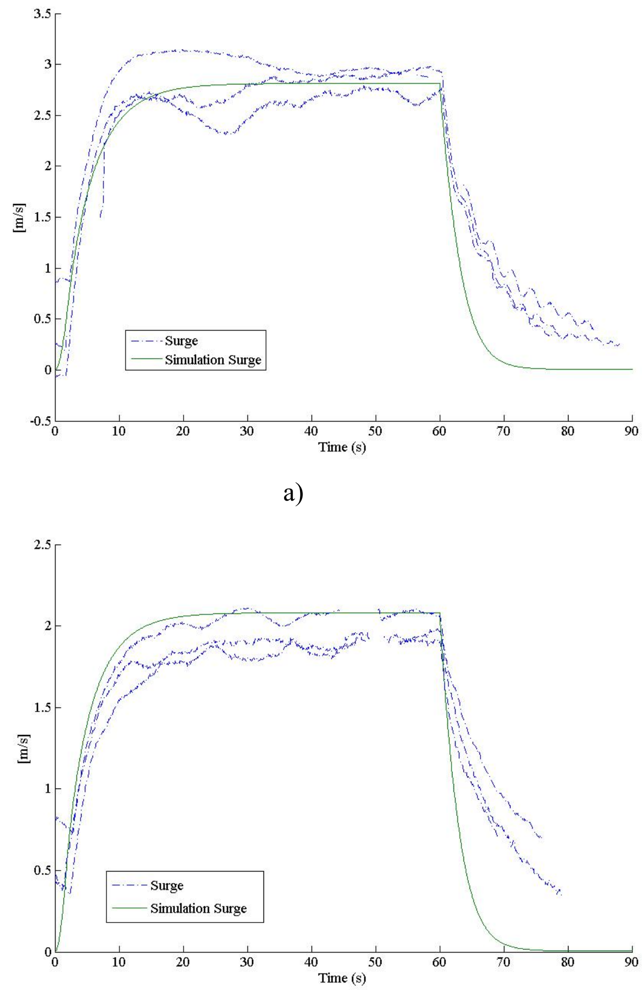

a)

b)

Figure 4. Acceleration test surge data for the lightship condition. a) 100%. b) 80%.

III. Initial Controller Design Results

After identifying and implementing the vehicle's mathematical model in Simulink, an initial controller was developed using a cascade of one Proportional Derivative (PD) heading controller and one Proportional (P) speed controller modified to incorporate a tolerance level for heading error. The tolerance level means that if the heading error is within a designated range (+/- 4 degrees) then no action is taken by the controller to correct it, and both motors will be given the same speed command intended to drive the vehicle at the reference speed.

The tolerance consideration is important for a vehicle steered via differential thrust because yaw rate and speed are highly coupled. For example, in order to execute a port turn, either the port motor speed must be decreased, the starboard motor speed increased, or both actions executed at the same time.

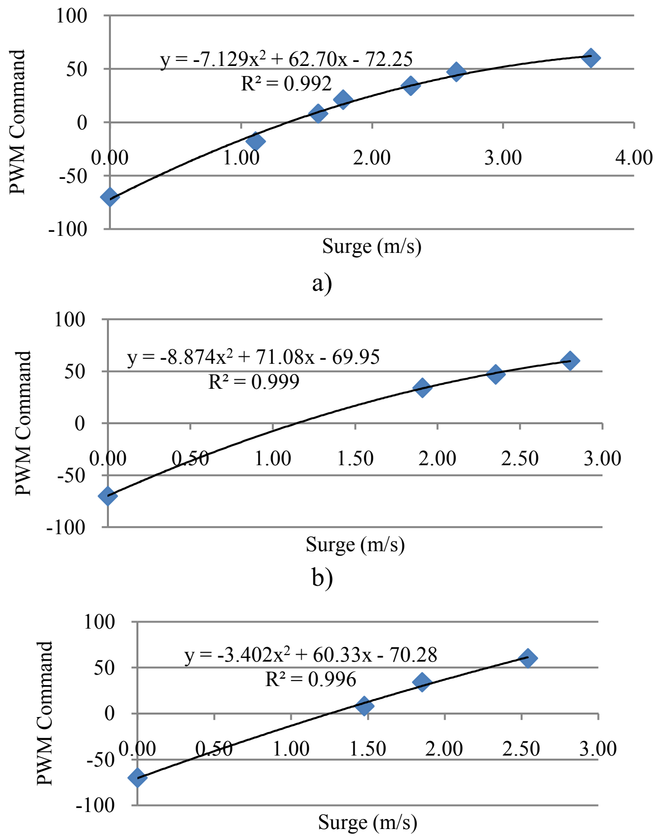

c)

Figure 5. Surge Axis Speed Curve Based on PWM Motor Command. a) Un-weighted. b) Lightship. c) Full Displacement

In each case, the ASV forward speed will change. This steering scheme is complicated further when the vehicle operates near its maximum speed and the only available action to initiate a turn is a decrease in speed of one motor, generating a speed loss. The control law for the vehicle under consideration prioritizes heading over speed control.

Results for the initial controller are shown in Table IV. Quantities of interest were the average magnitudes of speed and heading error for two reference speeds and the two mass configurations: an empty payload tray and with an approximate 25% addition of mass along the centerline of the vehicle. To approximate this payload addition the ASV mass, z-axis moment of inertia, draft, and forward hull drag were increased by 25%, and the longitudinal center of gravity was moved forward by 0.25 meters to reflect the positioning of the payload. The time-varying reference heading for this simulation is given by

$$\psi_{ref} = 45 + 45\sin\left(\frac{2\pi t}{20}\right), \quad (12)$$

where t is the simulation time in seconds, and ψ_{ref} is in degrees. The initial heading of the USV was set to 45 degrees with all other states zero.

Table IV. Cascaded PD/P controller performance

	Reference Speed (m/s)			
	1.5		3.5	
	$\overline{\lvert\psi\rvert}_e$	$\overline{\lvert u\rvert}_e$	$\overline{\lvert\psi\rvert}_e$	$\overline{\lvert u\rvert}_e$
Lightship	6.23	0.63	1.89	1.33
Lightship + 25%	36.4	0.80	31.1	2.52

[a] Yaw error in degrees and speed error in m/s

The cascade structure described above was the first implemented in simulation because of the desire to control the speed and heading of the USV under a known fixed mass condition. This serves as a starting point for more advanced controller design, which will be designed to adapt with the changing plant dynamics associated with an ALR.

IV. Conclusions

A three degree of freedom, physics-based model of a twin-hulled USV with waterjets was developed. An open-loop simulation was created to model a series of maneuvering tests. The same tests were conducted on the water with a WAM-V USV 14 under human operated remote control, and open-loop control from an onboard computer. Using the experimental results as a reference, the simulation parameters were tuned until the simulated output reasonably matched the experimental results.

An initial speed and heading control algorithm was implemented in simulation and control gain values were tuned for the case of constant reference speed and a sinusoidal reference heading.

To illustrate the deficiencies of a nonadaptive controller for the ALR mission, the same controller gains were used to simulate control of the ASV for an alternate reference speed, and also for different displacement configurations. The heading control performance decreased between the two displacement configurations for both speed commands, and speed control decreased more than 25% when the additional weight was added.

Although the PD cascade was able to control the USVs heading error moderately well at the original configuration, the speed did not reach the desired value in simulation. This problem was exacerbated when mass properties were changed.

The simulation results support the assumption that controller performance will not be the same for a plant with different dynamics (e.g. the USV drags an AUV through the water until it is lifted aboard). To remedy this problem the design of an adaptive controller that accounts for time-varying parameters is underway. The rate of time-variance is an important criterion for determining the method of adaptation. It is likely that a model reference adaptive controller will be developed for this class of vehicle. Robust terms will likely be needed to adjust quickly to abrupt system changes during the launch and recovery while the adaptive feature will adjust the control parameters needed for the lightship and AUV carriage conditions.

ACKNOWLEDGMENT

This work is supported by the U.S. Office of Naval Research under Grant N000141110926, Program Manager K. Cooper.

REFERENCES

[1] US Navy. "The Navy Unmanned Surface Vehicle (USV) Master Plan. 23 July, 2007.

[2] Freeman, D. K., "Remote delivery of unmanned systems technologies," *OCEANS, 2005. Proceedings of MTS/IEEE* , vol., no., pp.36,39 Vol. 1, 2005

[3] Chui, Kwan. "Autonomous Launch, Recovery and Servicing of UUVs from Unmanned Surface Vessels," Advanced Technology & Research Corp.

[4] "Underwater mobile docking of autonomous underwater vehicles," *Oceans, 2012* , vol., no., pp.1,15, 14-19 Oct. 2012.

[5] Slotine, Jean-Jaques E.; Li, Weiping, *Applied Nonlinear Control.* New Jersey: Prentice Hall, 1991.

[6] T. I. Fossen, *Guidance and Control of Ocean Vehicles*. Chichester: John Wiley and Sons Ltd, 1994.

[7] Sonnenburg, C.; Gadre, A.; Horner, D.; Kragelund, S.; Marcus, A.; Stilwell, D.J.; Woolsey, C.A., "Control-Oriented Planar Motion Modeling of Unmanned Surface Vehicles," *OCEANS 2010* , vol., no., pp.1,10, 20-23 Sept. 2010

[8] International Maritime Organization. *Explanatory Notes to the Standards for Ship Manoeuvrability*.16 Dec 2002. London.

[9] Sonnenburg, C.; Woolsey, C.A., "An experimental comparison of two USV trajectory tracking control laws," *Oceans, 2012* , vol., no., pp.1,10, 14-19 Oct. 2012.

[10] Sonnenburg, C.; Woolsey, C.A., "Modeling, Identification, and Control of an Unmanned Surface Vehicle," Journal of Field Robortics, vol. 30 iss. 3. May/June 2013. pp. 371-398.